

Polyelectrolyte adsorption at the solid-liquid interface favors receding contact line instability

Léa Delance,¹ Diego Díaz,² Arivazhagan G. Balasubramanian,² Outi Tammissola,²
Kaloian Koynov,¹ and Hans-Jürgen Butt¹

¹*Max Planck Institute for Polymer Research, Ackermannweg 10, 55128 Mainz, Germany*

²*KTH Royal Institute of Technology, SE-10044 Stockholm, Sweden.*

(Dated: 2 April 2026)

Controlling the motion of non-Newtonian drops on surfaces is crucial for applications ranging from inkjet printing to biomedical devices and food processing. While the macroscopic behavior of viscoelastic drops sliding on tilted hydrophobic surfaces has been characterized—showing reduced velocities and elongation compared to Newtonian fluids—the underlying microscopic mechanisms remain poorly understood. To address this gap, we developed a high-speed, high-resolution reflection microscope that enables direct visualization of the contact line of sliding drops. We used water-soluble polyelectrolyte solutions based on polyacrylamide and let drops sliding on hydrophobic substrates composed of Teflon AF- and PDMS-coated glass slides. The substrate tilting angle was varied between 20° and 45°. We reveal how viscoelasticity influences the dynamics of the receding contact line and drop motion. Our experiments demonstrate that viscoelasticity can destabilize the receding contact line, triggering filament formation. This instability previously observed in the coating of thin viscoelastic films, is reported here for the first time in sliding drops. We further highlight the critical role of polymer charge in this process: while cationic and non-ionic polymers promote filament formation, anionic polymers do not, a difference we attribute to the distinct wetting properties of the solutions. In conclusion, we clarify the interplay between rheology, surface interactions, and drop dynamics.

I. INTRODUCTION

Viscous fingering or Saffman-Taylor instability¹ is a well studied instability that arises when a less viscous fluid displaces a more viscous fluid, leading to the formation of "fingers". Fingering instabilities also occur at contact lines. For example, at advancing contact lines, when a fluid front is flowing down a tilted plate, regions with larger height flow faster leading to the formation of fingers². This instability is primarily driven by macroscopic flows, with contact line dynamics playing a minor role³. More recently, fingering instabilities have also been observed at receding contact lines in the context of non-Newtonian fluids, particularly viscoelastic fluids composed of an aqueous solution of high-molecular weight polymers⁴. The origin of this instability differs from that at advancing contact lines: it arises from the interplay between Van der Waals and capillary forces⁵. This results in a distinct dependency on contact line velocity. Unlike advancing contact lines, the wavelength of fingers forming at the receding contact line is found to increase with contact line velocity. However, this study does not account for fluid elasticity and does not explain the evolution of filament length with contact line velocity.

A drop sliding across a tilted plate provides a system that allows for the study of both advancing and receding contact lines. The literature on viscoelastic sliding drops is limited and primarily focuses on macroscopic features such as velocity and shape. Varagnolo *et al.*⁶ showed that sliding viscoelastic drops are elongated compared to Newtonian fluids, with the elongation depending on polymer flexibility and molecular weight. Xu *et al.*^{7,8} demonstrated the deposition of filaments at the rear of drops on superhydrophobic surfaces consisting of pillars. He linked their formation to the interplay between gravity, viscosity, and contact angle hysteresis. However, many aspects remain unclear: How do the physico-chemical properties of sliding drops affect contact line instabilities? Are polymers deposited on the surface during contact line motion? Understanding these questions is valuable for applications that rely on viscoelastic fluids of high molecular weight, including coating processes and transport of biological materials.

In this work, we explore the microscopic deformation of the receding contact lines of viscoelastic drops sliding across a hydrophobic surface. It turned out that viscoelastic sliding drops exhibit receding contact line instabilities leading to the formation of filaments. We demonstrate how the physico-chemical properties of the drop influence the onset of instability

and filament formation. We study polyacrylamide (repeat unit $-\text{CH}_2\text{CH}(\text{CONH}_2)-$) and two polyacrylamide-based polyelectrolytes. In these, a certain fraction of acrylamide units have been replaced by units bearing a non-zero charge in solution. When in solution, the anionic and cationic polyelectrolytes release their counter-ions and get charged. Polyacrylamide is generally considered to be non-ionic. As shown in⁹⁻¹¹, zeta-potential measurements indicate that Teflon AF surfaces acquire a negative charge and spontaneously form an electric double layer when exposed to water at neutral pH. We show that the occurrence of instability depends on the charge of the polymer in solution and is due to polymer/surface interactions. Cationic and non-ionic polymers are more prone to develop long filaments while anionic only show small deformation of the receding contact line. Finally, we demonstrate that these filaments lead to the deposition of polymer on the surface.

II. MATERIAL AND METHODS

A. Polymer solutions

Three polymers were used: polyacrylamide (FLOPAM FA 920 SH), non-ionic; a copolymer of acrylamide and acrylic acid (SNF, FLOPAM AN934 SH), anionic; and a copolymer of acrylamide and chloro-methylated monomer (SNF, FLOPAM FO 4290 SH). All polymers have high molecular weight ($5 - 15 \times 10^6$ g/mol) and are water-soluble. Solutions at 0.025% weight fraction were prepared by dissolving the polymer in milliQ water and stirring for two days until complete dissolution.

The shear-viscosity of the solutions was determined using a DHR-3 rheometer (TA Instruments) with a cone-plate geometry (2° angle). All fluids showed shear-thinning behavior, i.e, its viscosity decreased under applied shear rate (See supporting information, SI). The temperature was maintained at 25 ± 1 °C. The relaxation time τ of the solutions was determined using the Dripping onto surface method¹²⁻¹⁵. In this method, a drop was deposited on a surface and the thinning of the filament (liquid bridge) formed during deposition was recorded by a high speed camera at 5000 fps. The diameter of the filament was evaluated by ImageJ Software over time. The relaxation time τ was determined by fitting $\exp(-t/3\tau)$ ¹⁶ to the exponential thinning decay of the filament. The aspect ratio between the distance from nozzle to substrate (glass slide) H and nozzle radius r_0 was $H/r_0 = 3$.

The surface tension of the solutions was measured using the pendant drop method and was 71 ± 1 mN/m.

B. Surface preparation

The substrate consisted of glass slides with a thickness of 0.17 mm coated on the backside with a conductive ITO layer (Präzisions Glas & Optik GmbH). Two different hydrophobic surface coatings were prepared. Teflon AF-coated slides were fabricated by dip-coating the glass slides with a 60 nm layer of Teflon-AF from a 1 wt% Teflon AF at a withdrawal speed of 1 cm/min, followed by annealing at 160°C under vacuum for 24 h. PDMS-coated slides were prepared using a grafting-to method.¹⁷ The glass slides were drop cast with polydimethylsiloxane (PDMS) with a molecular weight of 6000 g/mol (Sigma Aldrich), placed into an oven at 100°C for 24 h, and subsequently rinsed with toluene and ethanol to remove free PDMS.

C. Reflection microscopy of sliding drops

We performed bottom-view imaging of contact line dynamics during drop sliding (Fig.1). An inverted epifluorescence microscope (Olympus IX83) was operated in reflection mode with a 20× objective (Olympus UCPLANFL N 20x) and a high-power LED (Thorlabs DC2200, 525 nm). The sample was placed on a grounded metallic stage modified using an objective inverter to allow for the observation of a tilted slide, as has been described in a previous article.¹⁸ Images were acquired at 10 000 fps using a high-speed camera (Photron, Phantom TMX 7510).

Reflection microscopy was combined with side-view imaging of the sliding drop using a second high-speed camera (Photron Fastcam Mini AX10, 125 fps) and a telecentric lens (Edmund Optics CobaltTL 0.274x). This enabled measurement of the macroscopic drop velocity and the advancing and receding contact angles θ_a and θ_r .

45 ± 3 μ L drops were formed from a grounded needle and allowed to slide on the studied hydrophobic surface. The microscope objective field of view was positioned at a distance of 2 cm from the beginning of sliding. For each drop both bottom-view and side-view images were recorded simultaneously.

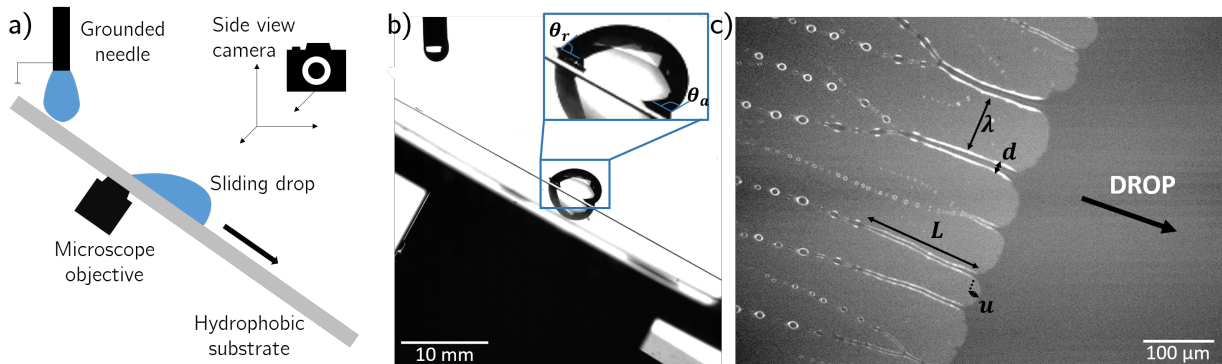


FIG. 1. a) Schematics of the setup used for reflection microscopy of sliding drops. b-c) Typical images obtained respectively from the side-view and bottom-view camera.

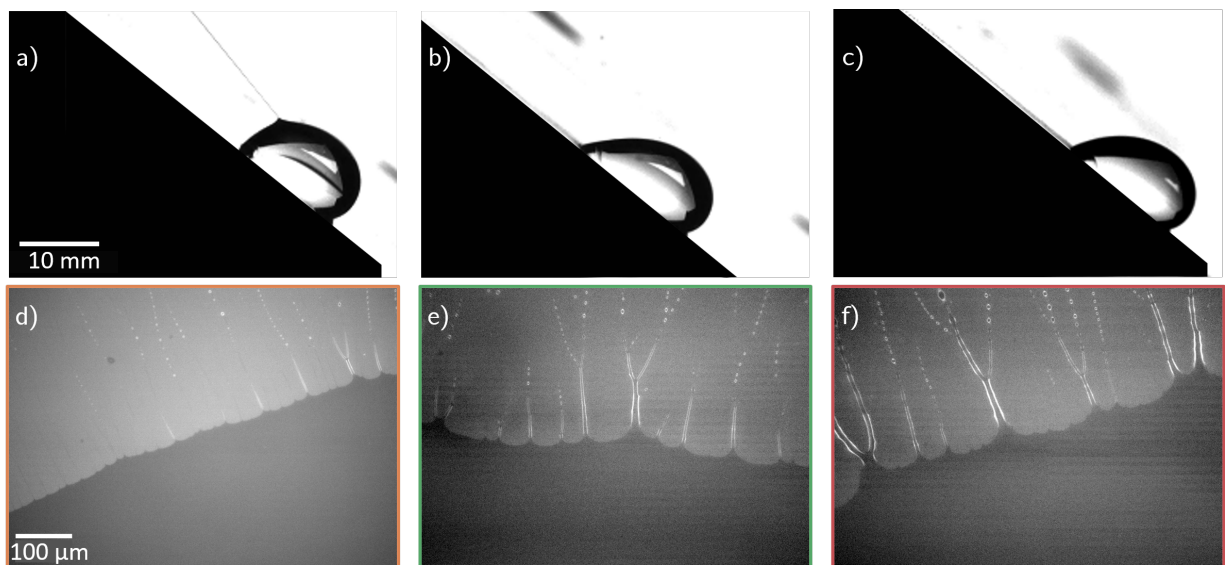


FIG. 2. Side-view images of the drops and reflection microscope images of the receding contact line for a tilting angle of 40° for the anionic polymer (respectively a,d), the non-ionic polymer (b,e), and the cationic polymer (c,f). The dark part correspond to a liquid/solid interface while the brighter part correspond to the air/solid interface.

After sliding, we checked the deposition of polymer using Scanning Electron Microscopy (ZEISS Gemini SEM 560). To do so, samples were coated after sliding with a 2.5 nm thick layer of platinum to avoid charging and were imaged with an accelerating voltage of 3 kV.

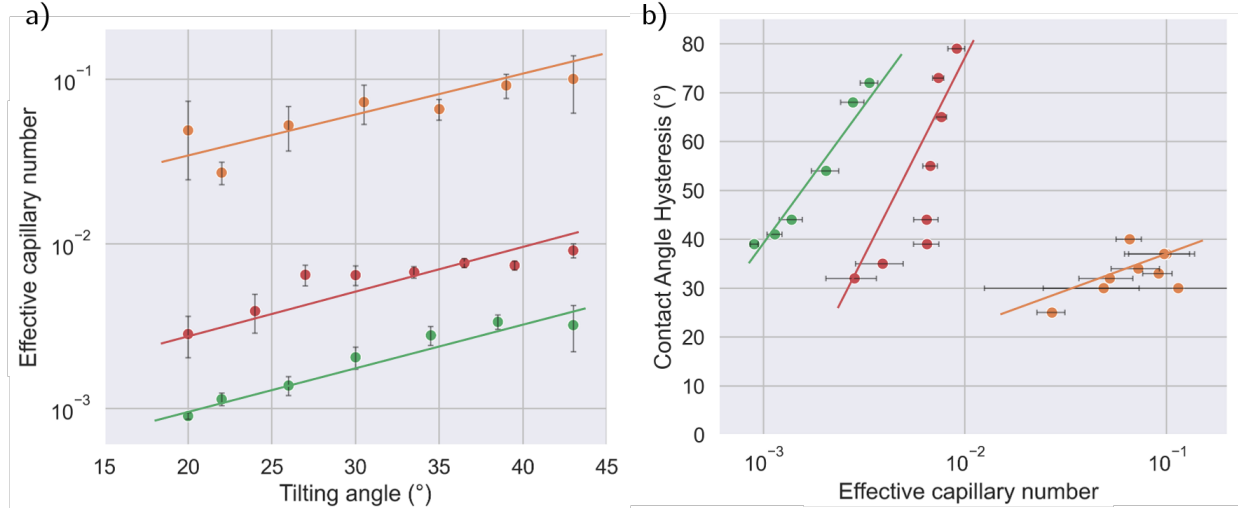


FIG. 3. (a) Effective capillary number as a function of the tilting angle and (b) contact angle hysteresis as a function of the capillary number for the anionic (orange), non-ionic (green), and cationic (red) polymers. Error bars were computed based on the standard deviation of the averaged velocity.

III. RESULTS AND DISCUSSION

For all solutions, side view (Fig. 2a-c) and reflection microscope videos (Fig. 2d-f) showed that the the advancing contact line (not shown) is smooth at the scale of $\approx 10 \mu\text{m}$ and exhibited no significant difference in shape from that of a pure water drop. In the following, we focus on the receding contact line. For the anionic polyelectrolyte (Fig. 2d), we observed small deformations of the contact line extending $u \approx 5 \mu\text{m}$ in the direction of sliding. The protrusions are associated with the formation of thin filaments ($d \approx 2 \mu\text{m}$ thickness). The protrusions are regularly spaced at $\lambda \approx 15 \mu\text{m}$ intervals but the formation of filaments is not continuous along the contact line: some protrusions did not result in filament formation. At lower tilt angles and thus lower speed, no filaments formed.

Cationic and non-ionic polymer drops (Fig. 2e,f) exhibited larger deformation (with an extension of $u \approx 20 \mu\text{m}$) and the formation of thicker ($d \approx 10 \mu\text{m}$), and longer filaments ($L \approx 100 \mu\text{m}$). The filaments destabilized at the end forming regularly spaced microdroplets. Filaments formed at every protrusion and were regularly spaced.

Drops containing the anionic polymer moved faster than non-ionic and cationic polymer drops. After sliding 3 cm the typical speeds were 30 to 60 mm/s for drops with dissolved

anionic polymer. The non-ionic and the cationic polymer drops slid with a velocity of roughly 5 to 50 mm/s and 1 to 10 mm/s, respectively. While cationic and non-ionic polymer drops reached a steady state velocity, anionic polymer drops were still accelerating after a slide length of 3 cm. In the following, we report the average velocity measured after a slide length between 2.5 and 3.5 cm.

To explore the reasons for the observed differences in the macroscopic motion, we performed rheology measurements (see Supplementary Information, Fig. S1) and found that the zero-shear viscosity of the polymer solutions differs with several orders of magnitude and that the solutions are shear-thinning. The zero-shear viscosities ranged from 0.009 Pa s (non-ionic) to 0.4 Pa s (cationic) and 4.9 Pa s (anionic). To account for these differences, we computed the effective capillary number $Ca = \eta_{eff}(\dot{\gamma})U/\sigma$, where η and $\dot{\gamma}$ are the characteristic viscosity and shear rate, respectively. Here, the characteristic shear rate is $\dot{\gamma} = U/D_0$ with D_0 as the drop diameter. The average drop velocity U was obtained from the side view images by measuring and dividing it by the corresponding sliding time. The viscosity η was determined from rheology measurements matching the characteristic shear rate with the steady shear curves (see SI). The surface tension σ is constant and indistinguishable from the one of pure water. We found that drops with anionic polymer have capillary numbers at least one order of magnitude higher than the non-ionic and cationic polymers (Fig. 3a). Therefore, after scaling with viscosity, we find that non-ionic and cationic polymer drops are slowed down compared to the anionic polymer. We later discuss the effect of polymer charge on drop sliding.

Given that the driving force for sliding (gravity) remained unchanged, this slowdown indicates an increase in friction force. The friction force experienced by a sliding drop is described using the Furmidge-Kawasaki equation^{19–22}:

$$F = w\sigma k(\cos \theta_r - \cos \theta_a) + F_{bulk}, \quad (1)$$

with w the drop width, $k \approx 0.8$ a geometrical factor, and $\theta_{a/r}$ respectively the dynamic advancing and receding contact angles. F_{bulk} is due to bulk viscous dissipation. Drop friction can therefore be quantified by measuring contact angle hysteresis, defined as $\Delta\theta = \theta_a - \theta_r$. We measured contact angles and $\Delta\theta$ for different tilting angles from side-view images at the moment the drop was observed with the microscope (Fig. 3b). We measured the receding contact angle using the macroscopic shape of the drop and ignoring the tails

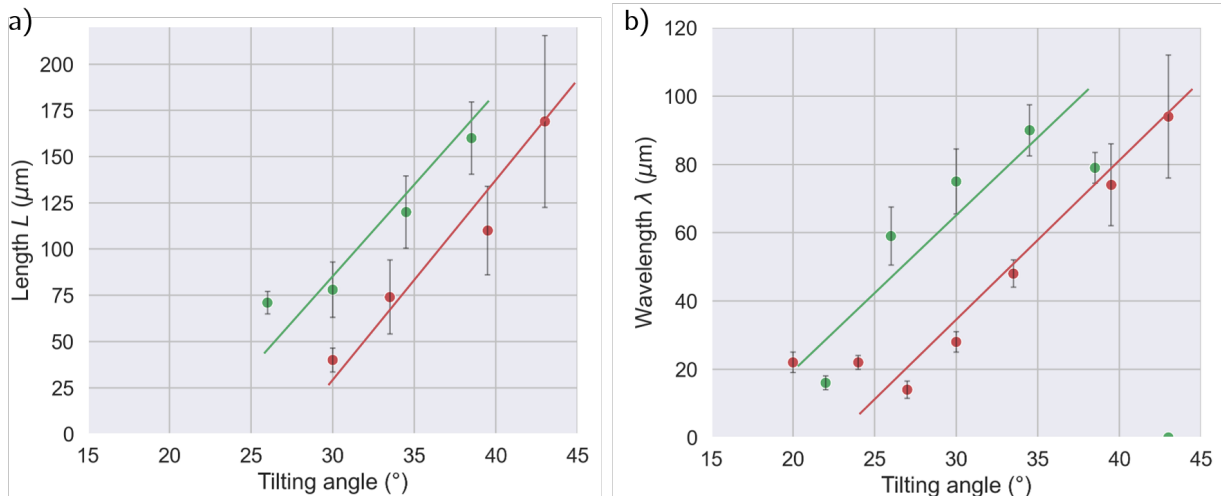


FIG. 4. (a) Length L and (b) wavelength λ of the filaments as a function of tilting angle for the non-ionic (green) and cationic (red) polymer. Error bars correspond to standard deviation.

observed for cationic and non-ionic polymer drops. Thus, the contact angles reported refer to the macroscale ($\leq 10 \mu\text{m}$) and can be considered apparent contact angles. For anionic polymer drops, the hysteresis remained stable (between 30 and 40°). In contrast, for non-ionic and cationic polymer drops, hysteresis increased and reached 70° for a tilt angle of 40° . This increase is primarily due to a decrease in the receding contact angle, while the advancing contact angle remains nearly constant. This reflects a higher friction for non-ionic and cationic polymers compared to the anionic polymer.

To further analyze the characteristics of the filaments as a function of tilting angle, we measured the average filament length L and average distance between filaments λ . For non-ionic and cationic polymers, L and λ increased with the tilting angle, reaching up to $175 \mu\text{m}$ and $90 \mu\text{m}$, respectively. The wavelength λ trend is consistent with previous studies, reported for a surface pulled from a liquid bath by Sharma *et al.*⁵ and blade coating by Deblais *et al.*⁴. Overall, our results demonstrate that viscoelastic sliding drops exhibit receding contact line instabilities, leading to regularly spaced filaments. Filament formation depends on drop velocity and polymer charge.

A. Hydrodynamics of viscoelastic wetting

The presence of polymers may alter drop motion and shape via two effects: either hydrodynamics (polymers rendering the solution viscoelastic and shear-thinning) or polymer-surface interaction. Let us first consider the hydrodynamics of viscoelastic wetting. For a Newtonian fluid, it is well-known from Cox-Voinov theory that the advancing (receding) contact angle increases (decreases) as the capillary number increases due to increased viscous stress. Accounting for hydrodynamics considerations, Kansal *et al.*^{23,24} and Bartolo *et al.*²⁵ showed that normal stresses arising from viscoelasticity only weakly affect the advancing contact line and contact angle but have strong effect on the receding contact line. It leads to a decrease in the receding contact angle compared to a Newtonian fluid. Regarding the advancing contact line, we indeed find no difference with that of pure water, neither with regard to the contact angle nor contact line smoothness. Moreover, we do observe a decrease in receding contact angle as we increase tilting angle and therefore capillary number. This increase is less than 10° for the anionic polymer drop, whereas it is more than 30° for the cationic and non-ionic polymer drops. Yet, the relaxation times of the solutions are 0.7 s for the anionic, 0.19 s for the cationic, and 0.04 s for the non-ionic polymer drop. From hydrodynamics considerations, we would therefore expect a stronger effect for the anionic polymer drop. As this is not observed experimentally, we conclude that polymer-surface interactions play an important role.

Regarding the triggering of the instability and filament formation, Sharma *et al.*⁵ theoretically show that a receding liquid film becomes unstable below a critical thickness. In Newtonian fluids, this leads to the emission of satellite droplets. In viscoelastic fluids, it results in filament formation: the elastic component (i.e., non-zero relaxation time) delays satellite droplet emission and make filament formation possible. However, they did not investigate how the filament characteristics (length, wavelength) depend on the solution. Yet, we observed significant differences in drop motion and contact line morphology depending on the polymer's charge. We now discuss the origin of these differences.

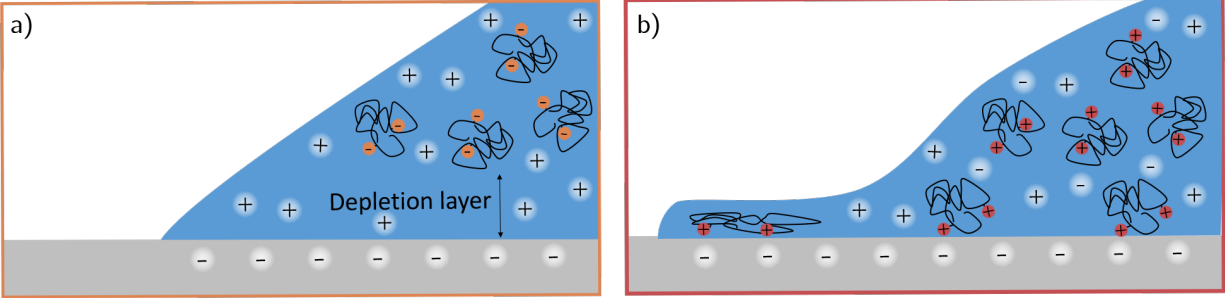


FIG. 5. Schematic of the rear side of a sliding drop representing polymer adsorption at the solid-liquid interface depending on its charge: (a) anionic and (b) cationic polyelectrolyte.

B. Effect of polymer charge

When discussing the interactions between the different types of polymers and the surface, we take into account that Teflon AF surfaces acquire a negative charge when exposed to water at neutral pH. Dissolved anionic polyelectrolytes are depleted near a negatively charge wall, as has been shown theoretically²⁶ and experimentally^{27,28}; i.e. a layer with lower polymer concentration is formed (Fig. 5). This is due to electrostatic repulsion between the surface and the polymer. The depletion layer has been measured for a similar polymer to be about 30 nm thick.²⁸ This is explained theoretically by balancing the monomer-wall interactions, which are repulsive in this case, with the osmotic pressure, which tends to homogenize polymer concentration. In terms of wetting properties, we therefore expect the static advancing and receding contact angles to be close to those of water, as well as a reduced viscoelasticity in the depletion layer.

In contrast to the anionic polymer, the cationic polymers adsorb on the surface²⁶, forming an arrested and stagnant region. We suggest that polymer adsorption reduces the solid-liquid surface energy, rendering the surface more hydrophilic, which leads to a higher drop friction and contact angle hysteresis.

In both anionic and cationic cases, we observe protrusions in the contact line. It shows that the liquid layer at the receding contact line has a thickness lower than the critical thickness determined in⁵. For the anionic case, we attribute the fact that no filaments are formed to the reduced elasticity in the depletion layer: the instability occurs but the oscillations are damped faster. In contrast, for the cationic case, polymer adsorption and solution elasticity favors filament formation.

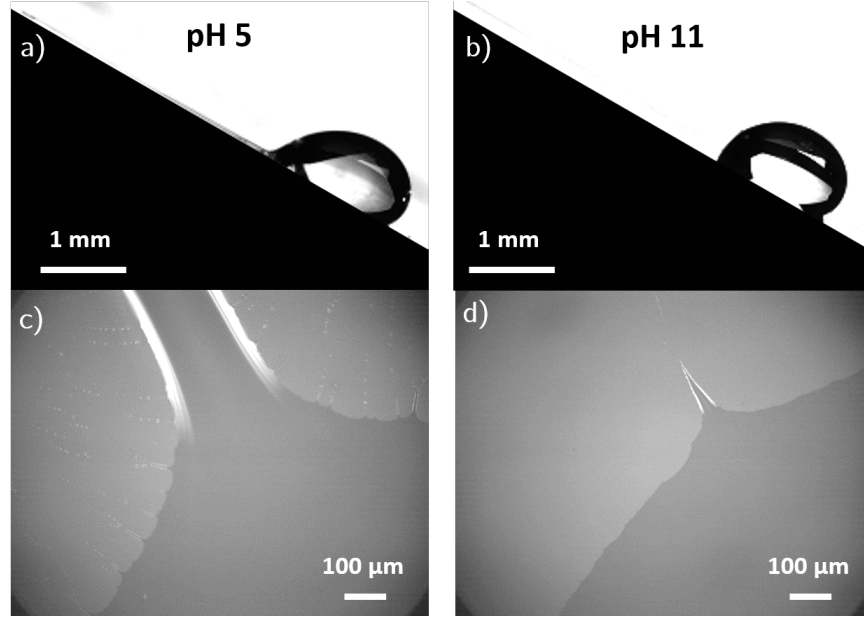


FIG. 6. Side (a-b) and bottom (c-d) view of the rear side of a moving drop at pH 5 and 11.

The formation of a depletion layer or of an absorbed layer also impact the liquid flow at the surface. For the anionic polymer a slip length is added while for cationic polymer the slip plane is shifted into the drop. However, these lengths are of the order of magnitude of the polymer radius of gyration. Compared to the size of the drop, this is negligible. We discuss later the evolution of the filament length over time as well as the deposition of polymer on the surface.

For the non-ionic polymer the situation is more complex. Polyacrylamide is considered to be neutral. Adsorption to the solid-liquid interface should not be enhanced by electrostatic interactions. Previous works have already demonstrated adsorption of polyacrylamide on silica surfaces²⁹. It had been explained by the formation of hydrogen bonds that, however, we do not expect on Teflon AF. To better understand an adsorption similar to cationic polymer, we study the effect of pH on the formation of filaments. Note that the initial solution has been made by mixing milliQ-water (at neutral or slightly lower pH due to CO₂ uptake) and the dry polymer. When dissolving polyacrylamide in water, we measured a pH of ≈ 8 . This observation indicates that polyacrylamide binds some hydronium ions, becomes protonated, and charges slightly positive. To validate this hypothesis, we performed experiments at pH 5 and pH 11. Changing the pH affects both the charge of the polymer and the Teflon AF surface. Nevertheless, for the range of pH tested, Teflon AF remains negative⁹. The new

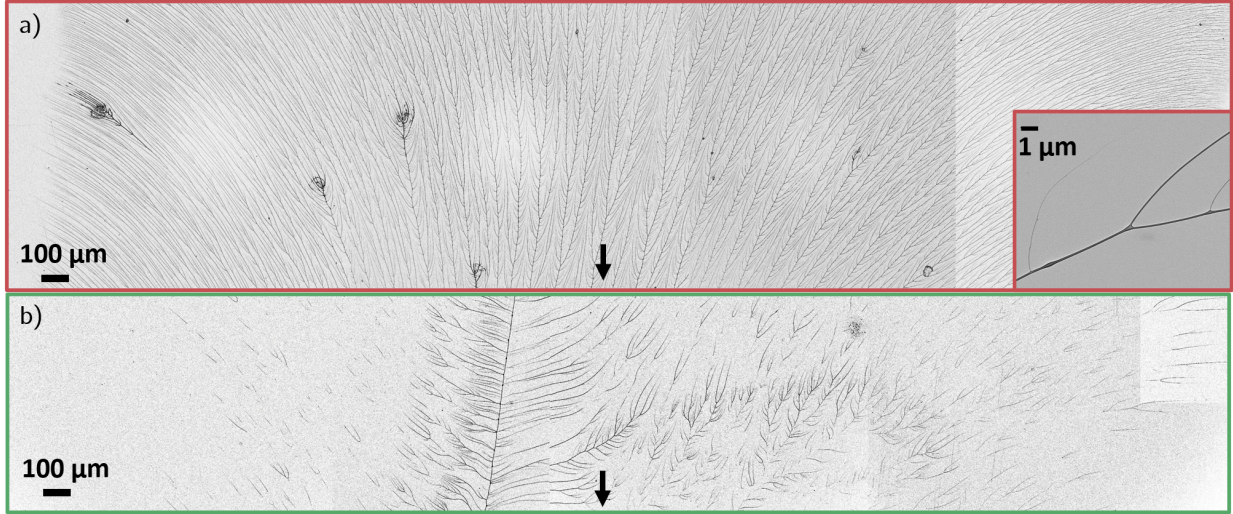


FIG. 7. Cationic (a) and non-ionic (b) polymer deposition observed by SEM after one drop sliding over the Teflon AF surface. Original SEM images have been analyzed using edge detection for better contrast. Black arrows indicate sliding direction.

solutions are prepared by adding respectively hydrochloric acid and sodium hydroxide to the initial solution. The volume added is small so that changes in polymer concentration remained below 5%. From the side view (Fig. 6a-b), we observe a difference in the receding contact angle of about 30° : $56 \pm 3^\circ$ at pH 5 compared to $86 \pm 3^\circ$ at pH 11. From the bottom view (Fig. 6c-d), we observe the formation of filaments and the deposition of microscopic droplets at low pH, that we do not observe at high pH. This confirms a stronger adsorption at low pH, for which we expect more amine groups to be protonated, than at high pH, for which we expect the polymer to be neutral.

At low pH, we also observe the formation of a tail of 2 mm length at the rear of the drop. This tail exists also at high pH but is only $100 \mu\text{m}$ long. This observation again indicates weaker adsorption. This tail is reminiscent of the pearling of sliding drops above a critical capillary number, studied in³⁰. However, in our case, the transition to pearling is due to a decrease in the receding contact angle rather than to an increase in speed. These results highlight the critical role played by polymer-surface interaction in triggering instability and filament formation. It is consistent with the idea that adsorbed polymers decrease the contact angle, thereby modifying the solid-liquid surface energy.

C. Polymer deposition

In Fig. 2, we also observe the breakup of the filaments in microscopic droplets. This is due to the Rayleigh-Plateau instability³¹. But the microdroplets are connected by a thinner filament. These filaments and microdroplets further dry and we expect it to lead to the deposition of polymer on the surface.

To further verify the deposition of polymer, we image the surface across the whole drop width using Scanning Electron Microscopy (SEM) after the sliding of a single drop (Fig. 7). For the drop containing cationic polymer, we observed the deposition of polymer in the form of filaments with a well defined spacing in the direction of motion. Filaments are oriented with an angle of $\approx 45^\circ$ compared to the direction of motion. This reflects the different relative motion of the contact line on the side of the drop. In the case of drops with non-ionic polymer, we also observe deposition of polymer but it is more scarce and we do not observe a pattern of continuous filaments. Most of the deposition occurs along the tail observed at the rear of the drop. We attribute the deposition of polymer to its adsorption at the solid-liquid interface. The polymer may directly adsorb at the solid-liquid interface or first move to the air-liquid interface and later adsorb at the receding contact line³². For drops with anionic polymer, SEM images did not reveal any deposition except close occasional dust particles, which might have locally pinned the droplet (see SI, Fig. S2). Using SEM on Teflon AF surfaces the resolution is limited and we can not resolve single chains. Therefore, we cannot exclude that deposition occurs at even smaller scale. However, these results show that adsorption is stronger for the cationic and non-ionic polymers than for the anionic polymer. Additional experiments with pure glycerol droplets sliding on Teflon AF further highlight the role of polymer deposition. These droplets showed no filament formation at the rear (see SI, Fig. S3). Since glycerol has no affinity for Teflon AF surfaces, the contact line remains fully mobile, the receding rim stays smooth, and the instabilities required for filament formation never develop.

D. PDMS-coated glass

The aforementioned results are obtained for drops sliding on Teflon AF-coated glass slides. To test the generality of the results to other surfaces, we carried out experiments with drops

sliding on glass slides coated with PDMS brushes for a tilting angle of 30° . Like Teflon AF surfaces, PDMS-coated slides charge negatively in solution but, in contrast to rigid Teflon AF surfaces, PDMS-coated surfaces exhibit a liquid-like behavior³³. We find that drops are slower on PDMS surfaces: 9 mm/s in average for the anionic polymer drop (against 15 mm/s on Teflon AF) and 8 mm/s for the non-ionic polymer drop (instead of 14 mm/s on Teflon AF). For the cationic polymer, the drop remains pinned and does not slide at the macroscopic scale and on the timescale of a few tens of seconds, even when increasing the tilt angles to 90° . A possible explanation for the slower motion on PDMS-coated surfaces is that the droplet deforms the PDMS layer, leading to the formation of a capillary ridge. In contrast to a rigid substrate, this introduces an additional mechanism of energy dissipation, namely, viscoelastic dissipation within the PDMS layer¹⁷.

This higher affinity for PDMS is also reflected in the contact angles: the advancing contact angle decreases from 123° and 117° on Teflon AF to 110° and 111° on PDMS, respectively, for the anionic and non-ionic polymers. Similarly, the receding contact angle decreases from 89° and 63° on Teflon AF to 74° and 58° on PDMS, respectively, for the anionic and non-ionic polymers. At the receding contact line of the two other polymers (Fig. 8), we find similar qualitative shape: small deformation with few filaments for the anionic polymer drop and filaments of a $\approx 100 \mu\text{m}$ for the non-ionic polymer drop. Therefore, although the macroscopic behavior depends on the substrate, we find that the shape of the contact line mostly depends on polymer charge. These results confirm the major role played by polymer-surface interaction in the formation of filaments. Moreover, the bright fringes observed in Fig. 8 are interferences fringes, which are reminiscent of the decrease in receding contact angle.

E. Filament dynamics

To understand the role of viscoelasticity in the filament formation, we estimated the magnitude of capillary, viscous and elastic stresses for the case of the cationic polymer. In this case, sliding drops of diameter $D_0 \approx 4 \text{ mm}$ move at typical velocities $U \approx 10 \text{ mm/s}$. At the bulk scale, the characteristic shear rate of $\dot{\gamma} \approx U/D_0 = 2.5 \text{ s}^{-1}$, which matching this shear rate to the rheological curve of the cationic polymer at 2500 ppm concentration (see SI, Fig. S1) shows that the effective viscosity remains roughly four times smaller than the

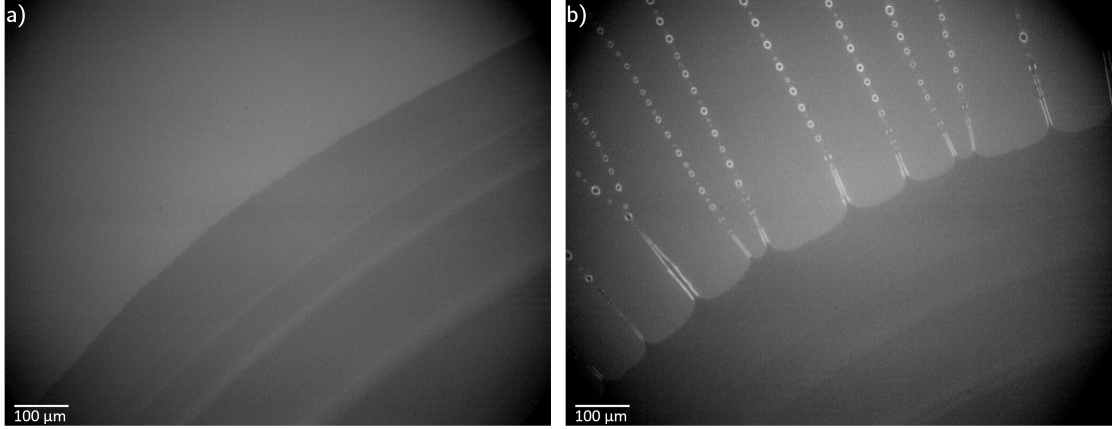


FIG. 8. Receding contact line on PDMS for a) anionic and b) non-ionic polymer drops imaged by the inverted reflection microscope.

zero-shear value. $\eta_{eff} \approx 0.1$ Pa s.

However, filament thinning is governed by uniaxial extensional flow, and the relevant resistance is set by the extensional viscosity η_E , not the shear viscosity. For a viscoelastic liquid under uniaxial extension, the extensional stress σ_{el} is¹⁶:

$$\sigma_{el} = \tau_{zz} - \tau_{rr} = \eta_E \dot{\epsilon}, \quad (2)$$

where τ_{zz} and τ_{rr} correspond to the normal and radial stresses along the filament and $\dot{\epsilon}$ is the extensional rate from Dripping onto surface measurements:

$$\dot{\epsilon} = -\frac{2}{R(t)} \frac{dR}{dt}, \quad (3)$$

Here, $R(t)$ corresponds to the minimum filament radius ($d_{min}/2$) over time obtained from the DoS high-speed recordings, assuming a cylindrical shape. The extensional viscosity can be expressed from the capillary balance as

$$\eta_E = -\frac{\sigma}{2 dR(t)/dt}. \quad (4)$$

Our DoS measurements shows a maximum of $\eta_E \approx 260$ Pa s and $\dot{\epsilon} = 4.5$ (Fig. 9), giving an elastic stress $\sigma_{el} \approx 1$ kPa. At the initial filament width $e_0 = 15 \mu\text{m}$ the capillary stress is $\sigma_{cap} = 2\sigma/h = 9.6$ kPa. This is about one order of magnitude larger than σ_{el} . Despite such difference, elastic stresses are sufficient to sustain filaments and slow thinning, allowing the formation of multiple beads separated by finite tails/filaments (Fig. 8). As thinning proceeds σ_{cap} increases with $1/h$, eventually overcoming σ_{el} to induce breakup.

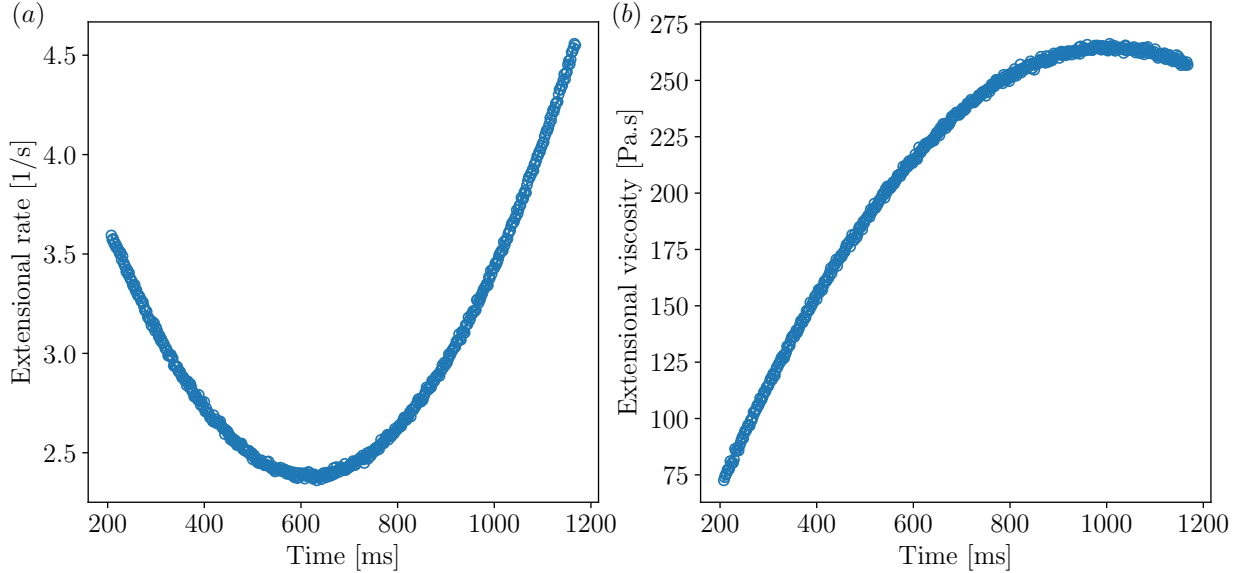


FIG. 9. Extensional rate (a) and (b) extensional viscosity for the anionic polymer.

Viscous stresses can be estimated as $\sigma_{vis} = \eta_{eff} \dot{\gamma}_{fil} = 2.6$ Pa, which are quite small in comparison with σ_{el} and σ_{cap} . Therefore, viscous stresses are negligible as instantaneous tensile resistance strength. Their role is rather dissipative, damping the growth of capillary perturbations. The bead on a tail morphology is thus a result of a Rayleigh-Plateau instability modified by the viscoelasticity, where capillarity drives the process elasticity sustain filament formation and delays breakup, while viscosity governs viscous dissipation. Note that the filaments observed in the “tail on a bead” instability are not stable. Following the argument of Xu et al.^{7,8}, we compare the breakup time of a viscoelastic filament, $\tau_b \sim \eta_E d / \sigma$, with a convective timescale $\tau_c = l / U$, where l is a characteristic length along the tail. Taking $L = w$, the experimentally observed bead spacing, and using $d \approx w / 2$, we obtain a critical extensional viscosity for the filament survival $\eta_E \sim 2\sigma / U \approx 14.4$ Pa s. This value is consistent with our observations: the extensional viscosity as determined from DoS is larger than this threshold, and the filaments, although they clearly form, break up rapidly after only a few bead spacings. In contrast to previous studies on micropillared superhydrophobic surfaces, where the bead spacing is constrained by the pillar pitch and filaments are anchored on pinned droplets^{7,8}, the spacing in our experiments is not imposed by surface topography (PDMS and Teflon AF are smoother). Instead, it reflects the intrinsic wavelength selected by the Rayleigh-Plateau instability, whose growth is delayed by viscoelasticity but

not suppressed.

IV. CONCLUSION

Our study demonstrates that viscoelastic sliding drops exhibit receding contact line instabilities, which lead to filament formation. The onset and extent of this instability depend critically on the charge of the polymer: cationic and non-ionic polymers promote the formation of long filaments, whereas anionic polymers show minimal deformation of the contact line. This behavior can be attributed to electrostatic interactions at the solid–liquid interface, leading to polymer adsorption in the case of cationic systems and depletion for anionic ones. Notably, the polymer initially classified as non-ionic was found to be partially protonated and to adsorb onto the surface, behaving similarly to cationic polymers. These findings emphasize the interplay between rheology, surface interactions, and drop dynamics, with potential applications in coating, printing, and surface engineering.

ACKNOWLEDGMENTS

The authors would like to thank Andreas Hanewald and Gunnar Glasser respectively for rheology and SEM measurements, as well as Lin Jian for providing the PDMS-coated samples. We also thank PolyChemie GmbH for providing the polymers used in the study. This work was supported by the European Research Council (ERC) under the European Union’s Horizon 2020 research and innovation program (Grant agreement No. 883631) (H.-J. B.).

V. AUTHOR DECLARATIONS

The authors have no conflicts to disclose.

VI. DATA AVAILABILITY

The data that support the findings of this study are available from the corresponding author upon reasonable request.

REFERENCES

- ¹P. G. Saffman and G. I. Taylor, “The penetration of a fluid into a porous medium or hele-shaw cell containing a more viscous liquid,” **245**, 312–329 (1997), publisher: Royal Society.
- ²H. E. Huppert, “Flow and instability of a viscous current down a slope,” **300**, 427–429 (1982), publisher: Nature Publishing Group.
- ³M. P. Brenner, “Instability mechanism at driven contact lines,” **47**, 4597–4599 (1993).
- ⁴A. Deblais, R. Harich, A. Colin, and H. Kellay, “Taming contact line instability for pattern formation,” **7**, 12458 (2016), publisher: Nature Publishing Group.
- ⁵S. Sharma and D. I. Wilson, “Newtonian and non-newtonian thin films create finite-time filaments: Experiments and theory,” **10**, 074003 (2025), publisher: American Physical Society.
- ⁶S. Varagnolo, D. Filippi, G. Mistura, M. Pierno, and M. Sbragaglia, “Stretching of viscoelastic drops in steady sliding,” **13**, 3116–3124 (2017), publisher: The Royal Society of Chemistry.
- ⁷H. Xu, A. Clarke, J. P. Rothstein, and R. J. Poole, “Sliding viscoelastic drops on slippery surfaces,” **108**, 241602 (2016).
- ⁸H. Xu, A. Clarke, J. P. Rothstein, and R. J. Poole, “Viscoelastic drops moving on hydrophilic and superhydrophobic surfaces,” **513**, 53–61 (2018).
- ⁹R. Zimmermann, S. Dukhin, and C. Werner, “Electrokinetic measurements reveal interfacial charge at polymer films caused by simple electrolyte ions,” **105**, 8544–8549 (2001), publisher: American Chemical Society.
- ¹⁰V. Tandon, S. K. Bhagavatula, W. C. Nelson, and B. J. Kirby, “Zeta potential and electroosmotic mobility in microfluidic devices fabricated from hydrophobic polymers: 1. the origins of charge,” *Electrophoresis* **29**, 1092–1101 (2008), <https://analyticalsciencejournals.onlinelibrary.wiley.com/doi/pdf/10.1002/elps.200700734>.
- ¹¹T. Preočanin, A. Selmani, P. Lindqvist-Reis, F. Heberling, N. Kallay, and J. Lützenkirchen, “Surface charge at teflon/aqueous solution of potassium chloride interfaces,” *Colloids and Surfaces A: Physicochemical and Engineering Aspects* **412**, 120–128 (2012).

- ¹²J. Dinic, Y. Zhang, L. N. Jimenez, and V. Sharma, “Extensional relaxation times of dilute, aqueous polymer solutions,” *ACS Macro Letters* **4**, 804–808 (2015).
- ¹³J. Dinic, L. N. Jimenez, and V. Sharma, “Pinch-off dynamics and dripping-onto-substrate (dos) rheometry of complex fluids,” *Lab on a Chip* **17**, 460–473 (2017).
- ¹⁴J. Dinic and V. Sharma, “Macromolecular relaxation, strain, and extensibility determine elastocapillary thinning and extensional viscosity of polymer solutions,” *Proceedings of the National Academy of Sciences* **116**, 8766–8774 (2019).
- ¹⁵B. P. Robertson and M. A. Calabrese, “Evaporation-controlled dripping-onto-substrate (dos) extensional rheology of viscoelastic polymer solutions,” *Scientific Reports* **12**, 4697 (2022).
- ¹⁶G. H. McKinley, “Visco-elasto-capillary thinning and break-up of complex fluids,” (2005).
- ¹⁷X. Zhou, Y. Wang, X. Li, P. Sudersan, K. Amann-Winkel, K. Koynov, Y. Nagata, R. Berger, and H.-J. Butt, “Thickness of nanoscale poly(dimethylsiloxane) layers determines the motion of sliding water drops,” *Advanced Materials* **36**, 2311470 (2024), <https://advanced.onlinelibrary.wiley.com/doi/pdf/10.1002/adma.202311470>.
- ¹⁸Y. Xiang, B. Straub, D. Cortes, H.-J. Butt, and K. Koynov, “When contact lines remember: Surface charge and the evolving interaction with defects,” *Droplet* **5**, e70039 (2026), <https://onlinelibrary.wiley.com/doi/pdf/10.1002/dro2.70039>.
- ¹⁹C. Furmidge, “Studies at phase interfaces. i. the sliding of liquid drops on solid surfaces and a theory for spray retention,” *Journal of Colloid Science* **17**, 309–324 (1962).
- ²⁰K. Kawasaki, “Study of wettability of polymers by sliding of water drop,” *Journal of Colloid Science* **15**, 402–407 (1960).
- ²¹H.-J. Butt, R. Berger, J. De Coninck, and R. Tadmor, “Drop friction,” **7**, 425–438 (2025).
- ²²G. McHale, S. Janahi, H. Barrio-Zhang, Y. Wang, J. Chen, G. Wells, and R. Ledesma-Aguilar, “Adhesive forces in droplet kinetic friction on liquidlike surfaces,” **135**, 204003 (2025).
- ²³M. Kansal, V. Bertin, C. Datt, J. Eggers, and J. H. Snoeijer, “Viscoelastic wetting: Cox–voinov theory with normal stress effects,” **985**, A17 (2024).
- ²⁴M. Kansal, C. Datt, V. Bertin, and J. H. Snoeijer, “Viscoelastic wetting transition: beyond lubrication theory,” **234**, 3121–3139 (2025).
- ²⁵D. Bartolo, A. Boudaoud, G. Narcy, and D. Bonn, “Dynamics of non-newtonian droplets,” **99**, 174502 (2007), publisher: American Physical Society.

- ²⁶P. G. De Gennes, “Polymer solutions near an interface. adsorption and depletion layers,” **14**, 1637–1644 (1981).
- ²⁷B. Cross, C. Barraud, C. Picard, L. Léger, F. Restagno, and E. Charlaix, “Wall slip of complex fluids: Interfacial friction versus slip length,” **3**, 062001 (2018), publisher: American Physical Society.
- ²⁸G. Guyard, A. Vilquin, N. Sanson, S. Jouenne, F. Restagno, and J. D. McGraw, “Near-surface rheology and hydrodynamic boundary condition of semi-dilute polymer solutions,” **17**, 3765–3774 (2021), publisher: The Royal Society of Chemistry.
- ²⁹E. Pefferkorn, “Polyacrylamide at solid/liquid interfaces,” **216**, 197–220 (1999).
- ³⁰T. Podgorski, J.-M. Flesselles, and L. Limat, “Corners, cusps, and pearls in running drops,” **87** (2001), 10.1103/physrevlett.87.036102, publisher: American Physical Society (APS).
- ³¹A. Lindner and C. Wagner, “Viscoelastic surface instabilities,” *Complex and biofluids*, **10**, 712–727 (2009).
- ³²X. Zhou, Y. Ji, Z. Ni, J. G. Lopez, K. Peneva, S. Jiang, N. Knorr, R. Berger, K. Koynov, and H.-J. Butt, “Spontaneous charging from sliding water drops determines the interfacial deposition of charged solutes,” *Advanced Materials* **37**, 2420263 (2025), <https://advanced.onlinelibrary.wiley.com/doi/pdf/10.1002/adma.202420263>.
- ³³S. Sbeih, A. Lüleci, S. Weber, and W. Steffen, “The influence of ions and humidity on charging of solid hydrophobic surfaces in slide electrification,” **20**, 558–565 (2024).